# NOTES AND CORRESPONDENCE

# Comparison of Two *Jason-1* Altimeter Precipitation Detection Algorithms with Rain Estimates from the TRMM Microwave Imager

N. TRAN, E. OBLIGIS, AND F. FERREIRA

*CLS, Division of Oceanography from Space, Ramonville St-Agne, France*

(Manuscript received 27 May 2004, in final form 22 November 2004)

ABSTRACT

This paper evaluates and compares the ability of two different *Jason-1* dual-frequency altimeter algorithms (referred as Tournadre's and Quartly's rain flags, respectively) to detect rain events in order to flag rain-contaminated altimeter range measurements. They are based on departures from a defined relationship between the Ku- and C-band radar cross sections observed in no-rain conditions. The algorithms' performances were assessed via collocations of these dual-frequency-based estimates with rain rates and a rain–no-rain flag from the Tropical Rainfall Measuring Mission (TRMM) Microwave Imager (TMI). The *Jason-1*–TMI analysis is built upon a yes–no discrimination, which is helpful in providing good insight into the altimeter rain detection flags' efficiency through estimations of the percentages of hits, misses, false alarms, and correct negatives when compared with TMI measurements. Tournadre's rain flag, based on a combination of altimeter and radiometer data, gives the best match with TMI estimates, compared to Quartly's, and also has a higher sensitivity to low-intensity rainfall.

## 1. Introduction

*Jason-1*, launched in December 2001, is a dual-frequency altimeter operating in the Ku and C bands, similar to its predecessor TOPEX. The primary reason for this dual-frequency choice was to allow direct correction for the propagation delay of radar pulses through the ionosphere by the use of the measurements themselves. Estimates of significant wave height and radar cross section are provided as separate values for each frequency and they were thought initially to be redundant.

As altimeter measurements over the oceans become increasingly accurate, the need for better correction and for better flagging of incorrect data could no longer be ignored. Results from previous studies on TOPEX data (Quartly et al. 1996; Tournadre and Morland 1997; Tournadre 1998; Quartly 1998) have shown that the effects of rain on all geophysical variables measured by an altimeter remain the least well understood of the different atmospheric perturbations that affect the measurements. Nowadays, no reliable correction of this contamination can be provided whether in the retrieval of the dynamic topography of the oceans or in the determination of wind speed (derived from the radar cross section) and surface wave height. The data possibly affected are simply discarded, using the setting of a flag.

The *Jason-1* proposed rain flags benefit from earlier research on TOPEX and rely on a criterion based on the detection of significant attenuation of the Ku-band backscatter coefficient versus the C-band one. Indeed it was shown by Quartly et al. (1996) and Tournadre and Morland (1997) that rain flags, based on this approach, provide good editing of the contaminated data. At this time two algorithms are proposed for *Jason-1*. They are, respectively, presented in Tournadre (2004) and in Quartly (2004) and will be referred as the JT and GQ algorithms hereafter.

This paper provides, first, a brief presentation of both algorithms and discussion on where the algorithms differ to identify sources of potential discrepancies in performances. Second, an assessment of the rain detection ability and sensitivity of each algorithm is per-

*Corresponding author address:* Ngan Tran, CLS/DOS, 8-10 Rue Hermes, 31526 Ramonville St-Agne, France.
E-mail: tran@cls.fr

formed. This was done by comparing *Jason-1* data with collocated data (surface rain rate) from an instrument dedicated to measure precipitation: the Tropical Rainfall Measuring Mission (TRMM) Microwave Imager (TMI). The results from this analysis gives insight into the efficiency of each algorithm by assessing whether all rain-affected data are flagged or whether good data are falsely discarded due to incorrect rain detection. The performance of each of the *Jason-1* algorithms will be evaluated via categorical statistics (yes–no/dichotomous discrimination) in terms of percentage of hits, misses, false alarms, and correct negative cases when comparing with TMI estimates. This information on the occurrence of events will be very useful for a quantitative comparison of the two *Jason-1* algorithms. There have been two previous exercises to validate such altimeter-based rain flag algorithms for TOPEX against independent rain datasets. Cailliau and Zlotnicki (2000) compared the TOPEX rain screening to Special Sensor Microwave Imager (SSM/I) data, while McMillan et al. (2002) compared it with various ground-based radar network data.

The analysis performed is laid out as follows. An overview of the two algorithms and discussion on where the algorithms differ are provided in section 2. Section 3 presents global comparison results between the two rain flag settings in term of percentage of data flagged over time and geographical patterns and their seasonal cycles, while section 4 focuses on the validation of the flags using independent TMI rain information. Section 5 wraps up the analysis with conclusions.

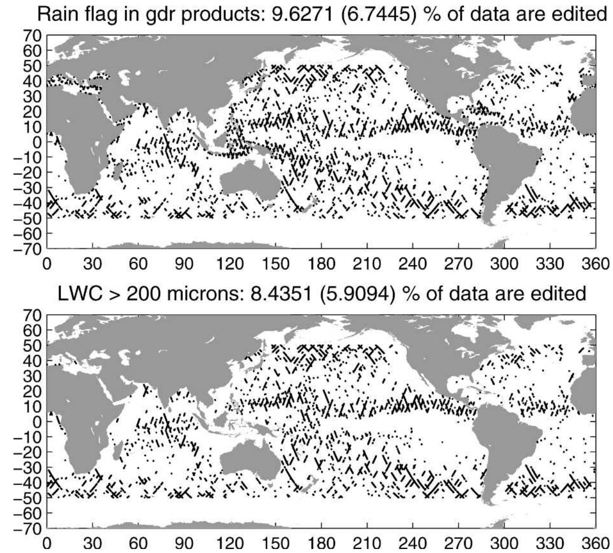


FIG. 1. (a) Location of rain cases identified by the rain flag in the current GDR product. (b) Data edited by a threshold on *Jason-1* LWC over cycle 23.

## 2. Rain flag algorithm description

Currently in the *Jason-1* Geophysical Data Record (GDR) products, the rain flag provided was derived from TOPEX measurements by Tournadre and Morland (1997). It is based on the combination of a criterion on the altimeter radar cross sections and a threshold on liquid water content (LWC) value estimated by the *Jason-1* microwave radiometer (JMR). A first take at this rain flag shows that its use leads to an edit of about 10% of the data within a cycle. Comparatively a flag, based only on JMR data, leads to an edit of about 8.5% of the data (as shown in Fig. 1) when using a liquid water path (LWP) threshold of at least 200 $\mu$m to point out any possible rainy situations. Note that a liquid water path of 1 mm is equivalent to 1 kg m$^{-2}$ of liquid water content (mass of water column per unit area). Note also that the TOPEX rain flag provided in the merged GDR generation B products is based only on the radiometer LWP and was not intended to detect rain. It solely indicates where the algorithm used to estimate water vapor would likely break down due to the presence of liquid water in the atmosphere as it was recalled by Cailliau and Zlotnicki (2000). The TOPEX rain flag is set when the liquid water path is larger than the threshold value of 600 $\mu$m. It has since been shown that this flagging recovers too few rain events and was not accurate enough for the screening of the altimeter data. These problems were mainly the result of the larger radiometer footprint size (about 4 times bigger that the footprint of the altimeter) leading to differences in sensitivity. Indeed the radiometer-derived measurements take into account features off the subsatellite track (not seen by the altimeter) leading to the editing of a large amount of the altimeter data from false alarms. It was then pointed out that a combined altimeter and radiometer measurements–based flag provides the best match for the detection of rain events. This was asserted from an analysis based on climatological precipitation data with an LWP threshold of 100–200 $\mu$m (Tournadre and Morland 1997; Cailliau and Zlotnicki 2000). With the advent of the availability of *Jason-1* data to users (cycle 1 corresponding to 16 January 2002), Tournadre (2004) and Quartly (2004) have adapted their respective TOPEX rain flag algorithms to *Jason-1* data. Please refer to their respective papers for details on the screening of the data that they used to determine their empirical Ku- and C-band radar cross-sectional relationships in the absence of rain. The principle that drives such developments is that rain-affected measurements do not conform to a well-defined empirical relationship between the dual-frequency measurements produced by the wind effect alone. Indeed through attenuation of the signal (reducing the backscattering) and also through damping of small-scale waves (increasing the backscatter cross section that can be considered as negligible in comparison to the attenuation effect), rain alters altimeter measurements. Due to the fact that the attenuation effect is frequency dependent and an order of magnitude smaller at C band than at Ku band, the knowledge of the relationship "free" of rain is therefore very useful for direct flagging of the altimeter rain-contaminated data.

### *a. Tournadre's rain flag*

Tournadre's rain flag is set if the measured Ku-band radar cross section is significantly attenuated when compared to the Ku-band value expected from the measured C-band one; that is,

$$\Delta\sigma_0 = f(\sigma_0^C) - \sigma_0^{\mathrm{Ku}} > A,$$

where $f$ is the Ku- and C-band "rain free" relationship and $A$ is an attenuation threshold. This latter value has been set to be equal to 1.8 times the rms of the $f$ relation with a minimum attenuation limit fixed at 0.5 dB [i.e., $A = \min(1.8 \times \mathrm{rms}, 0.5\ \mathrm{dB})$]. Note values are slightly different from Tournadre's paper (2004). They are from the specification sheet provided to the altimeter ground processing facilities for operational use (J. Tournadre 2004, personal communication). The $f$ function is a table defined for C-band radar cross-sectional values between 0.1 and 50 dB by a 0.1-dB step. In addition to this criterion, Tournadre also advocates the usefulness of testing for the presence of liquid water within the atmosphere by selecting the JMR cloud LWC greater than a threshold fixed here at 0.2 kg m$^{-2}$ (or LWP at 200 $\mu$m). This is done to eliminate possible false alarms especially at low speeds (i.e., high values of radar cross section) for which the backscatter variability is very high. *Jason-1* interim GDR (IGDR) data from cycles 2–28 have been used to tune the algorithm (table). The Ku- and C-band relation and its varying rms were estimated by binning the C-band data and by computing the mean and standard deviation of the corresponding Ku-band backscatter coefficient values. The atmospheric corrections were removed from the IGDR radar cross sections before the processing of this rain flag algorithm since these corrections include cloud liquid water effects and thus compensate for rain effects in some proportion. The number of measurements flagged by using simultaneously both criteria represents about 2% of the data per cycle.

### *b. Quartly's rain flag*

Quartly's rain flag has been evaluated using *Jason-1* GDR data from cycles 4 to 21. The radiometer-derived estimate of the atmospheric attenuation applied on the GDR radar cross-sectional measurement has been removed. As with the Tournadre algorithm, the tuning and subsequently its use are with the real observed values of the backscatter coefficients. Quartly's rain flag is also based on an attenuation threshold but not on the same quantity as is used by Tournadre. Here the rain flag is set if the derived attenuation between the Ku- and the C-band data are significantly different from the value provided by the mean relationship; that is,

$$\Delta\sigma_0 = (\sigma_0^{\mathrm{Ku}} - \sigma_0^{\mathrm{C}}) - g(\sigma_0^{\mathrm{C}}),$$

where $g$ is the mean relationship of $(\sigma_0^{\mathrm{Ku}} - \sigma_0^{\mathrm{C}})$ for a given C-band value. The proportion of data flagged, according to $\Delta\sigma_0 < -0.5$ dB, is about 1% per cycle. A table describing g for C-band values between 11.8 and 30 dB by a 0.05-dB step is used.

### *c. Comparison of the algorithms*

From the description provided above, we can see that performance discrepancies could be due to three potential sources. Differences could come from 1) slightly different mean relationships between $\sigma_0^{\mathrm{Ku}}$ and $\sigma_0^{\mathrm{C}}$, 2) different choices of thresholds, and 3) the incorporation or not of a JMR-based component. These issues have been previously discussed in different papers about means of determining the proper altimeter rain flag algorithm, and we synthesize here the conclusions to help readers get a global view and thus a better understanding of the results reported in the following sections.

Since the two equations for $\Delta\sigma_0$ are basically the same, with $g(\sigma_0^{\mathrm{C}})$ being $f(\sigma_0^{\mathrm{C}}) - \sigma_0^{\mathrm{C}}$, Fig. 2 shows these two terms in order to compare the Ku- and C-band mean relationships. Note that in the first release of the *Jason-1* IGDR products (cycles 1–45) a bias of $-2.26$ dB was added to the Ku-band backscatter coefficients and of $-0.28$ dB to the C-band values to make them consistent with TOPEX, but this has not been done for subsequent IGDRs or for the GDRs. So some adjustments were applied due to differences in the products used to determine these relationships. We can see afterward that the two curves, with respect to $\sigma_0^{\mathrm{C}}$, overlie one another closely over the $\sigma_0^{\mathrm{C}}$ interval of 12–22 dB. Note these curves have already been shown separately in the Tournadre (2004) and Quartly (2004) papers as Fig. 5a and Fig. 6, respectively, but they are reproduced here for a better reading of subtle differences between the mean relationships. For $\sigma_0^{\mathrm{C}}$ above 22 dB, the differ-

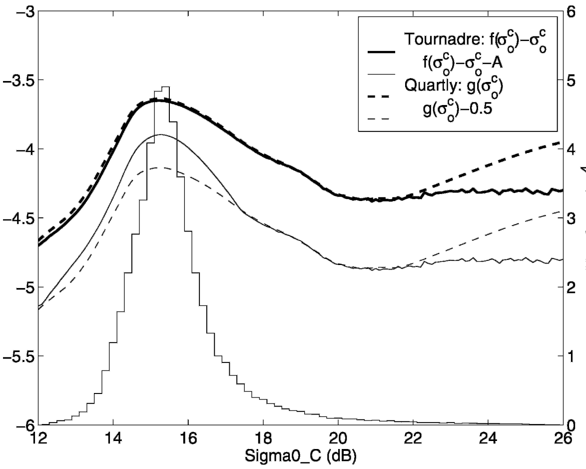


FIG. 2. Comparison of the two mean relationships (after adjustment of the $\sigma_0$ values since these relationships are derived from different disseminated products). They are presented as $f(\sigma_0^C) - \sigma_0^C$ and $g(\sigma_0^C)$. Also shown are the thresholds, i.e., $[f(\sigma_0^C) - \sigma_0^C - A]$ and $[g(\sigma_0^C) - 0.5]$, and the histogram of $\sigma_0^C$ over a cycle.

ence increases. However, as pointed out by Quartly (2004), for these very high $\sigma_0$ values (>20 dB), these relations have less significance as there are few points in each bin and the natural $\sigma_0$ variability is also high. Also provided in Fig. 2 are the plots of the two actual thresholds, that is, $[f(\sigma_0^C) - \sigma_0^C - A]$ and $[g(\sigma_0^C) - 0.5]$, and overlaid is the histogram of $\sigma_0^C$.

Since the two mean relationships are nearly identical over most of the $\sigma_0^C$ interval of values, the proportion of data flagged by either one of the algorithms depends upon the particular editing criterion used, that is, the threshold setting. Quartly (2004) already provides a report on the testing of these two types of thresholds (i.e., the difference in editing between using a specific attenuation value and one that relates the attenuation to a multiple of the varying measure of scatter) via his Fig. 6 and Table 2. Discussion of the relative merits of these two alternate choices was also provided earlier in Quartly et al. (1999). As we can observe in Fig. 2, the JT formulation gives greater sensitivity to moderate to high winds (low $\sigma_0$) than it does for low winds (high $\sigma_0$) with more of the data edited, whereas the GQ formulation was designed to give equal sensitivity across all wind regimes. Note that the data edited by both algorithms are not exactly the same for $\sigma_0^C$ above 17.5 dB (corresponding to wind speeds lower than 2.5 m s$^{-1}$) although the attenuation thresholds are identical because of the incorporation or not of a JMR component to help in reducing false flagging of points by confirming the presence of rain. In such calm conditions, factors other than rain may distort the $\sigma_0^{Ku} - \sigma_0^C$ relationship.

In summary, Quartly used a very conservative threshold to keep the percentage of flagged points low, while removing nearly all those believed to be contaminated by rain. His threshold of −0.5 dB was selected to optimize the elimination of bad altimeter data rather than for picking up the lightest rainfall. Stricter criteria, like that of Tournadre, pick out drizzle and light rain as we will see later on. This synthesis highlights the two different strategies that have been used: one focusing on discarding altimeter data likely to have been affected by rain and the other interesting in rain studies.

## 3. Comparison of edited data characteristics

Comparison of the two algorithms is performed with data from GDR files. Only the measurements between 50°S and 50°N have been considered (to avoid bad sea ice flagging) along with a criterion that ocean depth has to be greater than 1000 m to avoid any occurrence of land (coastal data). For these situations the rain flag might be set because of large differences between the backscatter coefficient values that would not be due to rain. This was used by Quartly to select valid ocean data; so in order to validate his rain flag in the best conditions we have to conform to his settings that allow for the optimum retrieved performance of the algorithm to compare the two rain flag algorithms. Note that no particular selection is mentioned in Tournadre's paper (2004) in addition to keeping good data with the usual data quality control requirements recommended by the *Jason-1* project team.

Figure 3 presents the spatial distribution of the edited data by the two algorithms from cycle 23. Tournadre's rain flag edits about 2% of the data while Quartly's algorithm edits less data, with only 1.5% flagged. The edited data draw similar patterns over the oceans that seem to be well correlated with regions where rain event occurrences are high. Note that the two distributions are not identical, with some areas highlighted by only one of the algorithm such as the Gulf of Mexico or the China Sea, for example. Figure 4 shows the same plots as in Fig. 3 but without the imposed restrictions on bathymetry and latitudes. The amount of data flagged at the limits of the sea ice extension near the Antarctic ice edge and along coastal areas, for instance in the Mediterranean Sea, the Red Sea, or the Hudson Bay, is not due to rain but may have other causes and should not be edited and related to rain events by the rain flag even if it is helpful to discard bad data due to bad sea ice flagging, for example. We think that a better option would be to have a rain flag truly associated with rain events with different levels of contamination with respect to rain rate (light, moderate, and heavy) and a

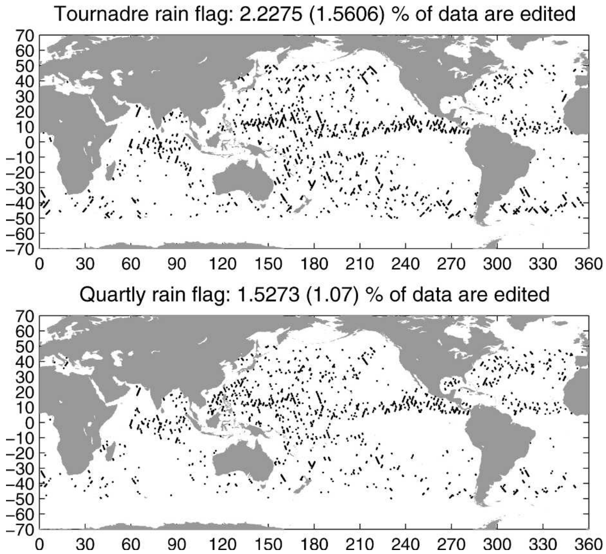


FIG. 3. Maps of data edited by the (a) Tournadre and (b) Quartly rain flag algorithms for the same GDR cycle 23 (filtering on bathymetry and latitude).

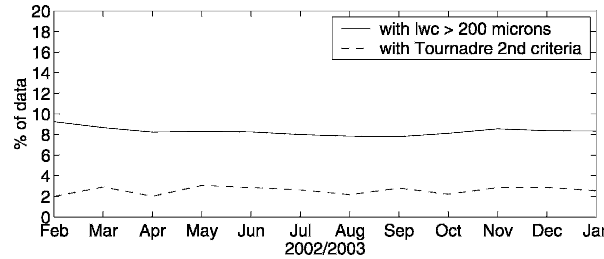


FIG. 5. Percentage of data edited by criterion on LWC or on radar cross sections in Tournadre's algorithm as function of time.

quality flag that could help to edit anomalous data whatever their causes (rain or others). Figure 5 shows that it is primarily the criterion on radar backscatter that drives the setting of the rain flag in the case of Tournadre's algorithm since the criterion on liquid water content would discard about 8%–9% of the data while the one on radar cross sections affects only 2% of the data. The percentage of edited data is rather stable as a function of time as shown in Fig. 6 for both algorithms. When the data are edited by the two algorithms simultaneously (i.e., edited when either one of the algorithms set the flag to one), we observed that about 50% of the edited data have been flagged by both algorithms (Fig. 7), and the other 50% are due to only one of the algorithms in the following proportion: 15% for the Quartly method and 35% for the Tournadre method, which is consistent with the fact that Tournadre's algorithm sets the flag for a larger number of situations as was seen previously.

Figures 8 and 9 allow the comparison of the spatial distribution of the seasonal rain event frequency of occurrences by the two algorithms (i.e., by summing the number of points for which the rain flag is set over a time period in a spatial box). The number of occurrences in each box of 2° latitude by 5° longitude has been normalized by the maximum number of points associated with a spatial box observed over all 2D histograms in order to have same color scale for all maps. Note that the color scale does not reach 1 because we saturate it for a better display of the features. We can observe good agreement between the maps over the same months especially in the tropical regions. Common features between the maps include a prominent rainbelt in the intertropical convergence zone (ITCZ); a dry zone in the midlatitudes of each hemisphere in the eastern Pacific, eastern Atlantic, and eastern Indian Oceans; and a wet area in the western parts of the three basins. These characteristics are in good agreement with existing rain climatologies (we are aware that pre-

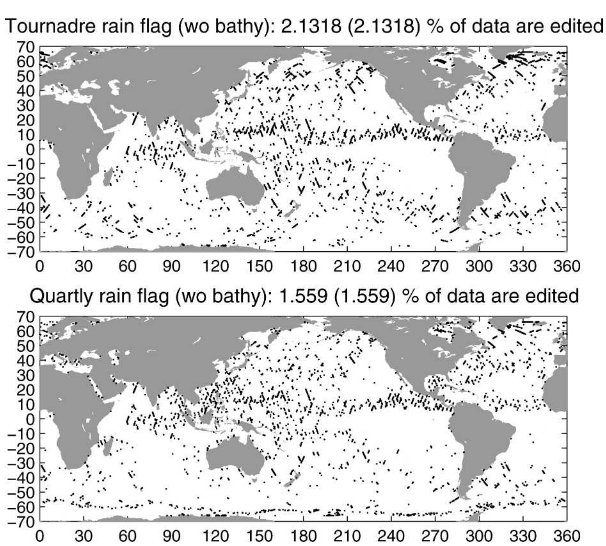


FIG. 4. As in Fig. 3, but without filtering on bathymetry and latitude.

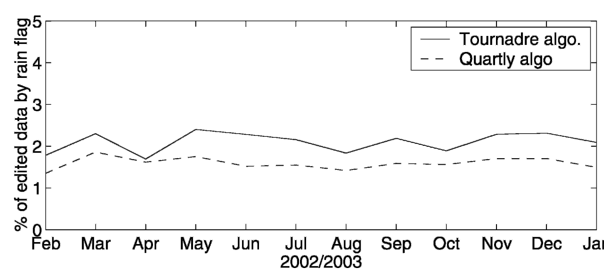


FIG. 6. Percentage of data edited by the Tournadre and Quartly algorithms as function of time.

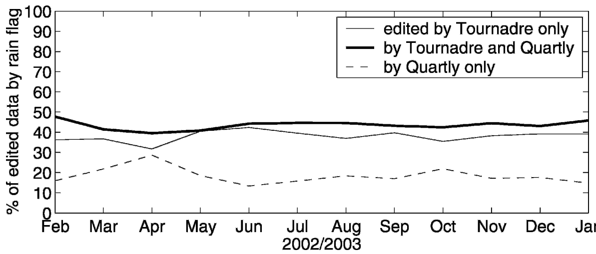


FIG. 7. Percentage of data edited as function of time (ratio of number of cases edited over the total number of data points edited when using both algorithms simultaneously).

cipitation maps show the intensity of the rain events while here we talk about the frequency of occurrences). But despite the overall similarity in the general patterns, it is also evident that the extents and areas of large numbers of occurrences of rain events are different between the two algorithms. In the tropical Pacific Ocean a stronger rainbelt is observed between 210° and 290° longitude in the Tournadre's maps. In the tropical Indian Ocean, the same maps suggest a less intensive rain zone off western Indonesia compared to the Quartly's maps while it is the opposite that is observed in the tropical Atlantic Ocean. Poleward of 20°S, one can observe three parallel rainbelts, respectively, extending southeastward from eastern Indonesia to the South Pacific, from Uruguay to the South Atlantic, and from the south of Madagascar to the south Indian Ocean. In the Northern Hemisphere, poleward of 20°N, two rainbelts are identifiable in the North Pacific and North Atlantic. All of these areas are better defined in Tournadre's maps than in those of Quartly since the rain flag associated with these latter maps is less often set at high latitudes. The seasonal variations in Quartly's maps show mostly variations in two areas: the tropical Indian Ocean and eastern Indonesia in the Pacific. These global comparisons show that the two proposed algorithms perform different screenings of the altimeter data and provide insight on their differences. To assess the reliability of each algorithm, we present in the next section results on the validation of both rain flags by comparison with independent rain data from the TMI instrument. We will only consider the precipitation detection aspect of the altimeter rain flags in the following.

## 4. Validation of the rain flags

### a. TMI data

The *TRMM* satellite was launched on 28 November 1997. The TMI on *TRMM* is a multichannel dual-polarized passive microwave radiometer. It utilizes nine channels operating at five frequencies between 10.7 and 85 GHz (dual-polarized measurements at all frequencies except 21 GHz, for which there is only a vertical polarized measurement provided) and provides data related to the rainfall rates over the oceans (Kummerow et al. 1998). It is similar to the SSM/I instrument in orbit on Defense Meteorological Satellite Program spacecrafts. Its effective fields of view depend on frequency, but they are elliptical and vary from 5 km × 7 km at 85 GHz to 63 km × 37 km at 10.7 GHz. However, data are delivered at cross-track intervals of about 5 km and along-track intervals of 14 km. Note that the altimeter radar cross-sectional sample represents an average over an area whose diameter is about 8 km or more and is larger when the wave height in the footprint is larger (Marth et al. 1993) and this is smeared by the ~6 km traveled in the nominal 1-s averaging period. So the filling of their respective footprints by a rain cell will be nearly identical if the time lag and distance between the pairing measurements are close to zero and comparable if the crossovers are close enough in space and time. The TMI uses a circular scan mode at an angle of incidence of 52.8°, resulting in a swath width of 759 km. Each scan begins with scene data measurements, followed by a cold reference measurement, and then a hot load reference measurement. These reference measurements, along with the known temperatures of the calibration loads, serve to calibrate the scan.

*TRMM* was designed to make measurements in the Tropics, but since the orbit was increased to 403-km altitude in August 2001 the swaths of TMI now cover the globe up to 39° of latitude. The *TRMM* standard data product 2A12 (the so-called TMI rainfall structure product) is used here in version 5, and it provides information on surface rain rate and a rain–no-rain flag. The principle behind the retrieval of these quantities is that the passive microwave sensor measures the brightness temperatures that are related to the vertically integrated hydrometeor amounts in the nine channels of TMI, which allows for the derivation of the surface rain rates. Note that the *TRMM* satellite data algorithms are being continually evaluated and improved by the TRMM science team and so the data in version 5 are for a period ending on 31 March 2004. Since 1 April 2004, version 6 algorithms are routinely used to process incoming *TRMM* data and existing data are reprocessed back to the start of the mission. Note that the change in the 2A12 product consists only of the additional computation of the latent heating and would not change anything for our analysis.

### b. Collocated dataset

The criteria used for the collocation between *Jason-1* and TMI crossovers are that time separation must be

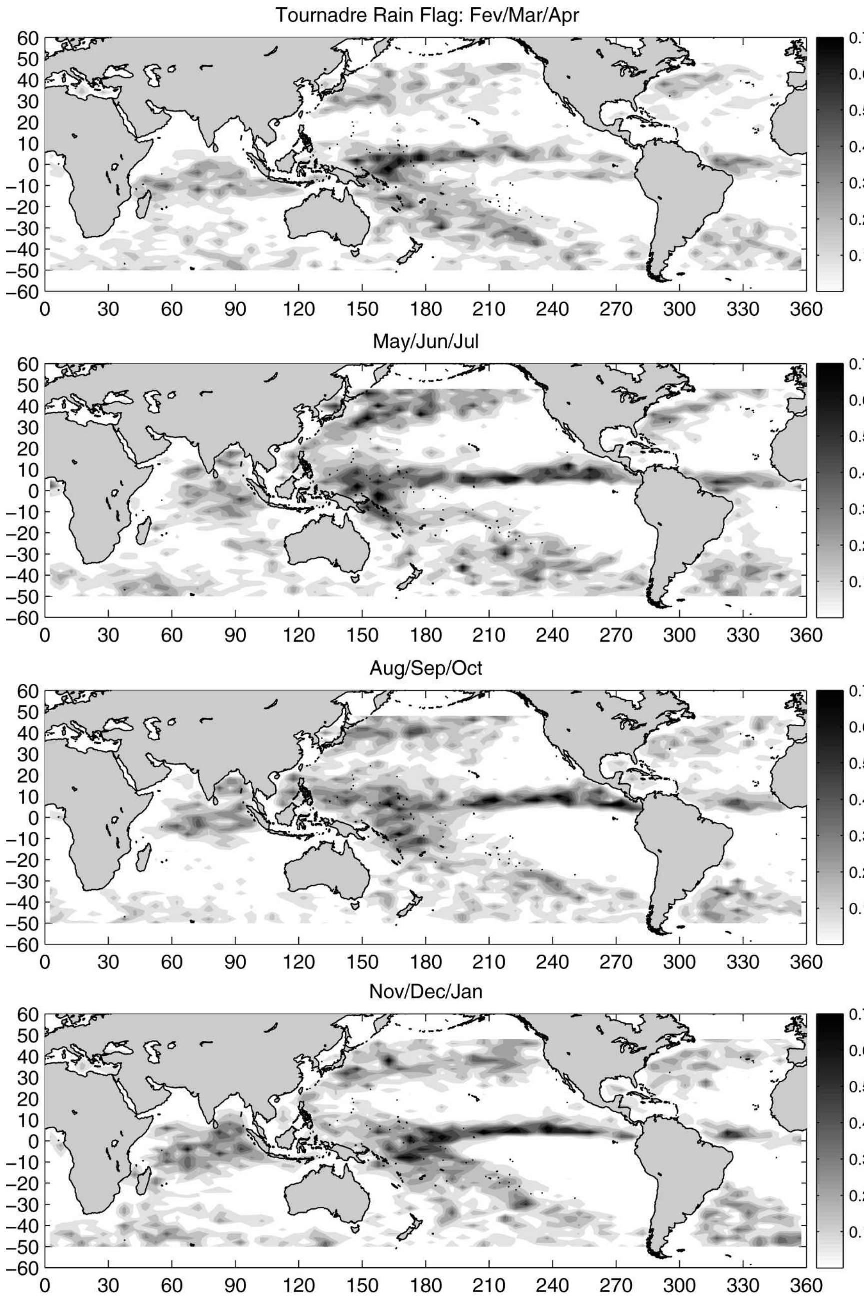


FIG. 8. Seasonal number of occurrences of rain events detected by Tournadre's rain flag in boxes of 2° latitude by 5° longitude (maps are normalized by the maximum number of occurrences found between maps in Fig. 9 and this figure).

within 30 min and spatial separation less than 50 km between respective observations. This would allow for reasonable comparisons of the two independent datasets. The principle behind the pairing of the data between *Jason-1* and TMI is that for each *Jason-1* measurement, we select measurements by TMI that match the time window, then among these measurements the closest one is selected if it matches the distance criterion; otherwise, there is no crossover. The collocation set spans a 1-month period, July 2002, leading to a total of about 47 000 crossovers. This number is limited in latitude to the Tropics within ±39° of the equator due to TRMM orbits, which is fine for our analysis because this area corresponds to regions where rain events are the most frequent. The collocated set allows for the evaluation of the *Jason-1* rain flags sensitivity for in-

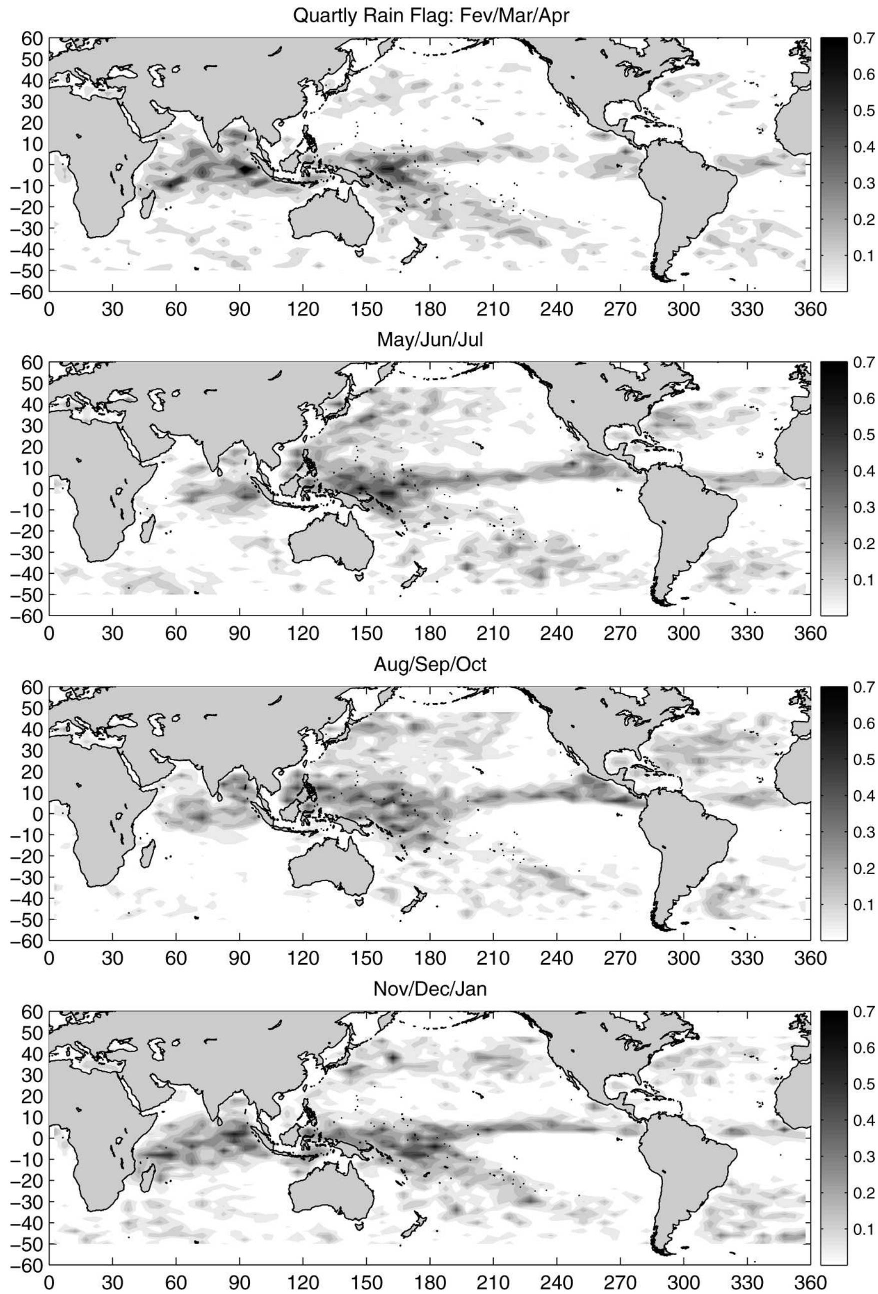


FIG. 9. As in Fig. 8, but for Quartly's algorithm.

stantaneous surface rain rates from 0.1 up to 20 mm $h^{-1}$. Note that a rain rate of 0.2–0.5 mm $h^{-1}$ represents roughly the limit of detectability of passive microwave radiometers. Ninety-seven percent of the TMI rain estimates fall at rain rates between 0.1 and 12 mm $h^{-1}$ as shown in Fig. 10 (the percentages provided are with respect to the total collocated dataset defined by the selection criteria, the low numbers indicate the low number of rainy situations); this percentage is reduced to 72% for rain rates between 0.5 and 12 mm $h^{-1}$. Figure 11 shows the spatial distribution of the crossovers. As can be seen, the crossovers are gathered as *Jason-1* track segments because both satellites are in prograde orbits with different orbital inclinations (at 35° and 66°, respectively, for TRMM and *Jason-1*). This causes configurations where *Jason-1* crosses all of the TMI swath during which successive measurements continuously satisfied the collocation criteria with different TMI data.

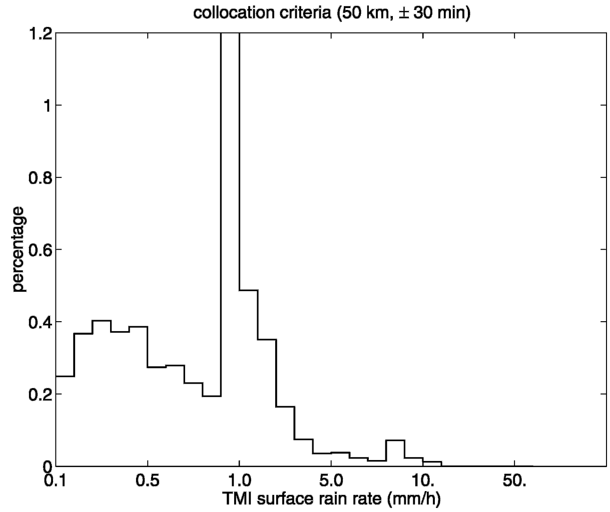


FIG. 10. Histogram of TMI-retrieved rain rates in the interval 0.1–50 mm $h^{-1}$ from the collocated dataset. For a clearer display of the histogram (due to the logarithmic interval of variation of the rain rate), the bar width represents an interval of 0.1 mm $h^{-1}$ between 0.1 and 1 mm $h^{-1}$, of 1 from 1 to 10 mm $h^{-1}$, and then of 10 above 10 mm $h^{-1}$.

## c. Intercomparison results

The analysis of this dataset shows that 5.54% of the crossovers have the TMI rain flag set while only 1.79% and 1.60% have the *Jason-1* rain flag set by, respectively, the Tournadre and Quartly algorithms. We plot these flagged data as a function of latitude in Fig. 12. The three distributions display similar tendencies, except for two latitude bands: latitudes higher than 30°S and between 12° and 4°S, where the peaks observed in TMI distribution are completely missed by both *Jason-1* rain flags. The TMI distribution shows a primary peak at 8°–10°N and a secondary peak at 6°–8°S. Around 20° in both hemispheres, it depicts a minimum number of occurrences of rain events and farther poleward it shows a local maximum in each hemisphere. These results point out that our limited collocated dataset is, however, large enough to display the major characteristics of the climatological rain distribution in the TMI rain event distribution.

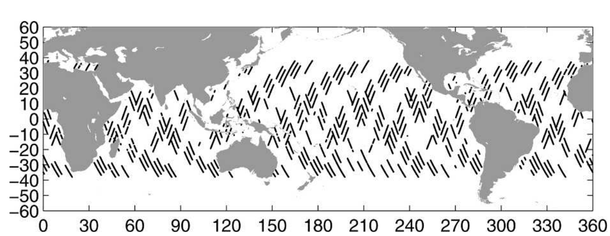

FIG. 11. Distribution of the crossovers between *Jason-1* and TMI.

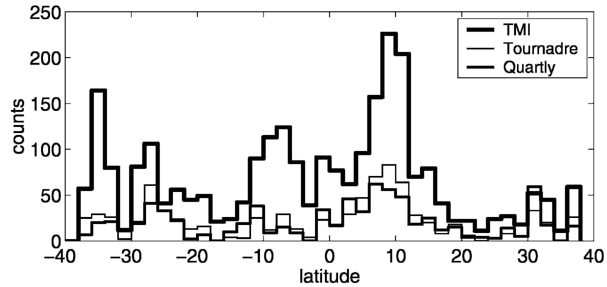


FIG. 12. Distribution of the data for which a rain flag has been set with respect to latitude for the collocated dataset.

The choice of a 30-min window and a 50-km interval allows for a sufficient number of collocated pairs between *Jason-1* and TMI to be obtained to provide statistically significant results, but a 30-min time window is long relative to the few minutes over which precipitation can change significantly and the 50-km interval is large relative to the horizontal extent of rain cells. As rain is highly sporadic in time and space (a tropical convective rain cell has a 10-km diameter on average and a duration of about 10 min), it is difficult to carry out remote sensing measurements of rain cells simultaneously. It is thus difficult to validate the comparison analysis without interpreting the effects of time difference and distance. Figure 13 provides the percentage of data as a function of both distance and time lag between the collocated pairs. We can see that 90% of the pairs are separated by less than 10 km so we should be able to refine the analysis by decreasing the selection criteria while keeping the results statistically significant. Table 1 presents the classical way of comparing a yes–no detection criterion to another one considered as "truth," which is, in our case, the TMI rain flag. The different quantities used for the evaluation are then the number of hits, misses, false alarms, and correct nega-

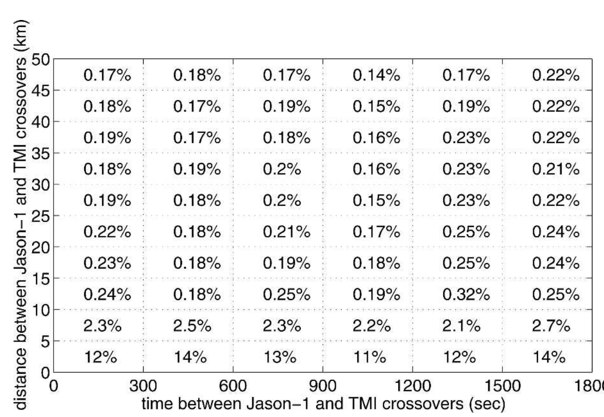


FIG. 13. Distribution of data as a function of both time lag and distance between crossovers.

TABLE 1. Yes–no discrimination definitions.

| Yes–no (dichotomous) discrimination | | TMI rain flag: Yes | TMI rain flag: No |
|---|---|---|---|
| *Jason-1* rain flag algorithm | Yes | Hits | False alarms |
| | No | Misses | Correct negatives |

tives. The event occurrences for evaluating the categorical statistics are given as a percentage of the actual compared pairs, which means that the percentage values are comparable in Table 2. Note that misses and false alarms cases can be due to the collocation criteria since a rain event of very small extent can be observed in the footprint of one sensor and not seen by the other because it was out of its own footprint.

The sensitivity of the results to temporal and spatial criteria of collocation is also addressed by computing the results for two more restrictive filters. The first one corresponds to a selection of crossover data characterized by a 15-min time separation and a distance of up to 10 km (about 22 000 crossovers remaining) while the second one selects a much smaller number of crossovers (361), with a time lag of up to 5 min and 1 km in distance. These tighter collocation criteria ought to provide better matching points with identical atmospheric conditions. These three comparison cases would help to compare the two *Jason-1* rain flag algorithms in order to select the best one for operational use. Table 2 shows that the percentage of correct negatives is always higher for the Tournadre algorithm than for the Quartly one, whatever the selection filter. For the Tournadre rain flag, the percentages of hits and misses are, respectively, higher and lower. Note also that the percentage of false alarms is null for this algorithm. All the results lead to the same conclusion; the Tournadre algorithm provides the best performances between the two algorithms proposed for the *Jason-1* mission with systematically closer agreement between this rain flag and the TMI one, if this latter point is considered as the truth, even when we lower the collocation criteria for a stricter comparison. These results corroborate previous observations by Cailliau and Zlotnicki (2000) who highlighted, in their independent validation of TOPEX rain flags, that an altimeter–radiometer-based algorithm performs better than an altimeter-only one.

Figure 14 displays the distribution of the *Jason-1* measurements that are considered to be hits, misses, and false alarms by comparing each *Jason-1* rain flag with the TMI one. No particular patterns can be observed for each group of data; they seem to be randomly distributed within the climatological rainfall patterns. Figure 15 gives the distribution of the occurrence of hits and misses as a function of the TMI surface rain-rate estimates from light to moderate rain events $<15$ mm h$^{-1}$ (there are too few samples with heavy rain events in this collocated dataset to draw conclusions in this case) for the two *Jason-1* algorithms, respectively, which can be interpreted as the sensitivity of each algorithm. This analysis provides insight into how the percentages of hits and misses in Table 2 are distributed versus TMI rain rates. These results reenforce the conclusion that Tournadre's algorithm is the more accurate. The plots associated with it show that the minimum detectable rain rate that triggers the flag is lower (about 0.5 mm h$^{-1}$) than that for Quartly's algorithm (about 1 mm h$^{-1}$). This minimum value provides an indication of the sensitivity of each algorithm and can be understood to be the so-called rain–no-rain threshold. The discrepancies between the two *Jason-1* algorithms almost certainly result from a difference in sensitivity due to the different thresholds used as discussed in section 2c.

The accuracy of the detection of light rain is much less than that for heavy rain. A deficit in the detection of light rain is revealed that gives rise to future developments. To follow this lead, in the Tournadre algorithm case we tested the relaxation of the constraint on liquid water path to different values of the threshold (50 and 100 $\mu$m). The liquid water content may not exceed the chosen threshold of 200 $\mu$m either because of the small size of the rain cell compared to the JMR footprint or because of the small impact in very light to light rain situations. Moreover, the altimeter samples

TABLE 2. Intercomparison between the two *Jason-1* rain flags settings when comparing with TMI rain flags.

| | $N$ (100%) | *Jason-1* algorithm vs TMI | Hits (%) | Misses (%) | False alarms (%) | Correct negatives (%) |
|---|---|---|---|---|---|---|
| 30 min/50 km | 47 374 | GQ | 1.09 | 4.45 | 0.54 | 93.90 |
| | | JT | 1.78 | 3.75 | 0.0 | 94.43 |
| 15 min/10 km | 22 027 | GQ | 1.13 | 3.64 | 0.59 | 94.64 |
| | | JT | 1.83 | 2.94 | 0.0 | 95.23 |
| 5 min/1 km | 361 | GQ | 0.55 | 0.83 | 0.28 | 98.34 |
| | | JT | 0.83 | 0.55 | 0.0 | 98.61 |

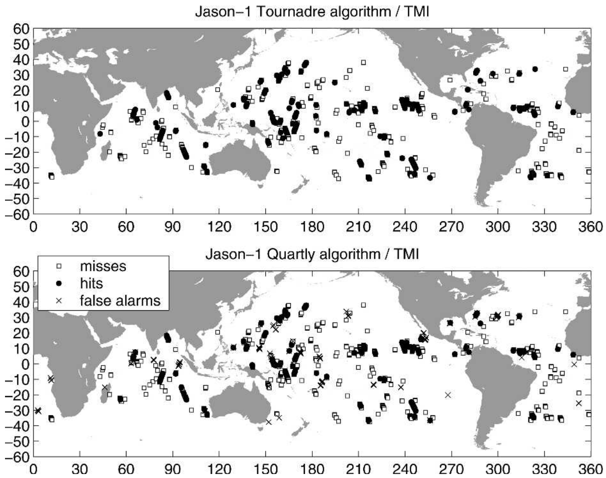


FIG. 14. Distribution of the *Jason-1* crossovers marked as hits, misses, and false alarms by using the Quartly or Tournadre rain flag algorithm with respect to the TMI rain flag.

are sensitive to smaller-scale variations than are the radiometer ones and so affected altimeter data might be undetected by such screening depending on the threshold used. Changing the LWP limit made no difference in the results because of the distribution of LWP values in the collocated dataset; while removing this criterion does not change the percentages of either the hits or misses (the ones that we were expected to improve), it does lowers the percentage of correct negatives and increases the percentage of false alarms from null to 0.55% in the (5 min, 1 km) collocation configuration. In the two other less restrictive configurations, the percentages of hits and misses improve at the cost of degrading the percentages of correct negatives and false alarms. The latter can be larger than the one observed with Quartly's algorithm.

In fact, the previous conclusions need to be qualified. As explained by Tournadre in his review of this analysis, the attenuation threshold of 0.5 dB corresponds to a rain rate of about 1–2 mm$^{-1}$. The detection of light rain (<1 mm h$^{-1}$) by altimetry is illusory since a 0.5 mm h$^{-1}$ rain rate and a 5-km rain thickness give 0.16 dB of attenuation. The latter result is comparable to the geophysical or instrumental radar cross-sectional variability and so it will not be detected by the criterion on the radar cross-sectional difference. Moreover, in general light rain does not lead to erroneous altimeter estimates of geophysical parameters and should not be discarded. As pointed out by Quartly (2004), a threshold of −0.5 dB is effective at removing the majority of the spurious data records from the *Jason-1* GDRs and it also appears to be useful for most applications since it discards less than 2% of the global data. According to a simple physical model, Quartly's rain flag type should trigger at 2.3 mm h$^{-1}$ (Quartly et al. 1999) to pick up significant rain events. The dedicated *Jason-1* algorithm performs better than that with lower detection sensitivity although the detection rate only reaches about 50% in the 3–4 mm h$^{-1}$ category.

## 5. Conclusions

We compared and evaluated the performances of two *Jason-1* rain detection flags, those proposed by Tournadre (2004) and Quartly (2004). These flags are not calibrated to recover precipitation rates but only to determine whether or not rain is present and has degraded the altimeter measurements. The main conclusion is that the Tournadre's rain flags are closer to the TMI ones with a lower sensitivity threshold than are those of Quartly. The results are as expected since the algorithms were established with different purposes; indeed, Tournadre's formulation attempts to use precipitation to detect flag-contaminated data while Quartly was thought to detect bad altimetric data, rain being one of the sources of degradation. The validation of the algorithms was performed only up to 39° of latitudes due to the *TRMM* orbits. However, the tropical area is the most representative for rain events so results found here are significant. Cailliau and Zlotnicki (2000) recalled that the zonally averaged profile of annual rain rate versus latitude shows a three-peak structure. The near-equatorial peak is the largest with 5.5 mm h$^{-1}$, centered around 5°N (the intertropical convergence zone), the secondary peaks are 3.5 mm h$^{-1}$ at 40°–50°S and 2.5 mm h$^{-1}$ at 40°–50°N, and precipitation at 70°N or 70°S is at most 1 mm h$^{-1}$. Rain is more frequent but less intense at high latitudes, and from the results reported here the efficiency of the *Jason-1* algorithms would be questionable at high latitudes due to the lower sensitivity of the detection of low rain rate, particularly for Quartly's algorithm. In fact in the framework of the altimeter mission, the purpose of the rain flag is not to flag all rain events but only the ones that can possibly have a negative impact on the altimeter estimates. Results show that the rain flag detection of the data affected (rain rate >1 mm h$^{-1}$) is better with Tournadre's algorithm than with Quartly's. From Fig. 15, it appears that for rain rates above 1 mm h$^{-1}$, the number of misses by Tournadre's algorithm is quite low. For rain rates above 2 mm h$^{-1}$, it is close to zero.

Finally, note that even if the monitoring of the radiometer products, and in particular the radiometer wet tropospheric correction, has pointed out different anomalous behaviors since launch (see, e.g., Obligis et al. 2004), the effect for the liquid water content threshold in Tournadre's algorithm is evaluated to be small

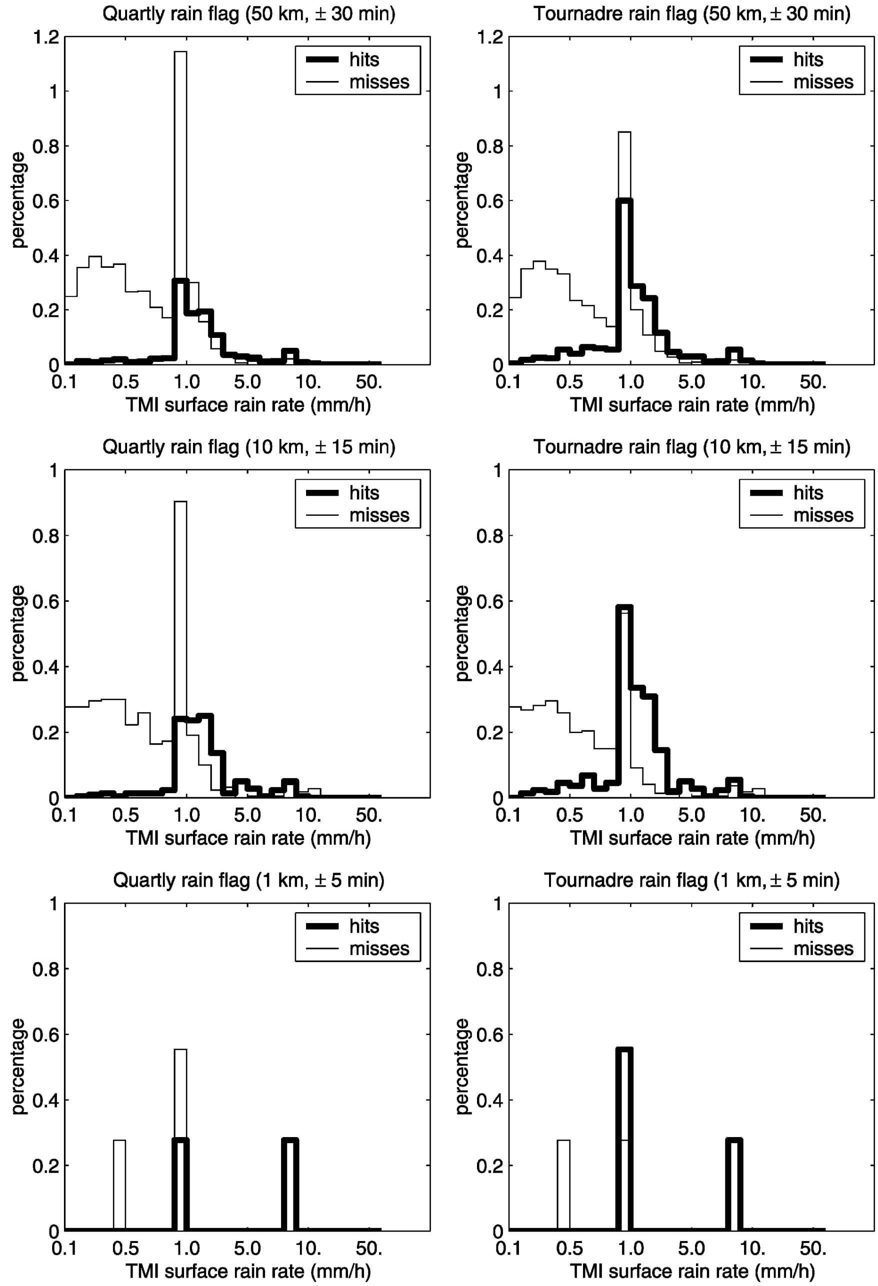


FIG. 15. Distribution of the occurrence of hits and misses as a function of TMI rain rates. For a clearer display of the histogram distributions (due to the logarithmic interval of variation of the rain rate), the bar width represents an interval of 0.1 mm $h^{-1}$ between 0.1 and 1 mm $h^{-1}$, of 1 from 1 to 10 mm $h^{-1}$, and then of 10 above 10 mm $h^{-1}$.

since the amount of data flagged by this criterion remains relatively stable over time as shown in Fig. 5. The observed incident was monitored between cycles 27 and 33 corresponding to October–November 2002 and there is no drastic change observed over this period in the plot. The month of July used for the collocation of *Jason-1* with TMI corresponds to cycles 18–20, and the *Jason-1* data over this period of time were used in the development of both rain flag algorithms, so we were in a good configuration to validate both algorithms.

*Acknowledgments.* The authors wish to thank Jean Tournadre and Graham Quartly for their very helpful reviews of the original paper. We would like also to acknowledge the straightforward and rapid electronic access to the TMI data at the Goddard Space Flight Center Distributed Active Archive Center. This work was performed under contract with the Centre National d'Etudes Spatiales (CNES), Toulouse, France.

## REFERENCES

Cailliau, D., and V. Zlotnicki, 2000: Precipitation detection by the TOPEX/Poseidon dual-frequency radar altimeter, TOPEX Microwave Radiometer, Special Sensor Microwave/Imager and climatological shipboard reports. *IEEE Trans. Geosci. Remote Sens.,* **38,** 205–213.

Kummerow, C. D., W. Barnes, T. Kozu, J. Shiue, and J. Simpson, 1998: The Tropical Rainfall Measuring Mission (TRMM) sensor package. *J. Atmos. Oceanic Technol.,* **15,** 809–817.

Marth, P. C., and Coauthors, 1993: Prelaunch performance of the NASA altimeter for the TOPEX/Poseidon project. *IEEE Trans. Geosci. Remote Sens.,* **31,** 315–332.

McMillan, A. C., G. D. Quartly, M. A. Srokosz, and J. Tournadre, 2002: Validation of TOPEX rain algorithm: Comparison with ground-based radar. *J. Geophys. Res.,* **107,** 4038, doi:10.1029/2001JD000872.

Obligis, E., N. Tran, and L. Eymard, 2004: An assesment of *Jason-1* microwave radiometer measurements and products. *Mar. Geod.,* **27,** 255–277.

Quartly, G. D., 1998: Determination of oceanic rain rate and rain cell structure from altimeter waveform data. Part I: Theory. *J. Atmos. Oceanic Technol.,* **15,** 1361–1378.

——, 2004: Sea state and rain—A second take on dual-frequency altimetry. *Mar. Geod.,* **27,** 133–152.

——, T. H. Guymer, and M. A. Srokosz, 1996: The effects of rain on TOPEX radar altimeter data. *J. Atmos. Oceanic Technol.,* **13,** 1209–1229.

——, M. A. Srokosz, and T. H. Guymer, 1999: Global precipitation statistics from dual-frequency TOPEX altimetry. *J. Geophys. Res.,* **104,** 31 489–31 516.

Tournadre, J., 1998: Determination of rain cell characteristics from the analysis of TOPEX altimeter echo waveforms. *J. Atmos. Oceanic Technol.,* **15,** 387–406.

——, 2004: Validation of Jason and Envisat altimeter dual frequency rain flags. *Mar. Geod.,* **27,** 153–169.

——, and J. C. Morland, 1997: The effects of rain on TOPEX/POSEIDON altimeter data. *IEEE Trans. Geosci. Remote Sens.,* **35,** 1117–1135.